Anisotropic charge transport in ion-conductive photoresponsive polyethylene oxide–based mesomorphic materials

Corinne Binet,[1,*] Alexandre Allart,[1] Patrick Judeinstein,[2,3] and Frédérick Roussel[1,†]

[1]*Université de Lille–Sciences et Techniques, Unité Matériaux et Transformations (UMET), CNRS, UMR 8207, UFR de Physique, P5, 59655 Villeneuve d'Ascq Cedex, France*

[2]*ICMMO, UMR 8182 CNRS-U. P-Sud, Université Paris-Saclay, Université Paris-Sud, 91405 Orsay Cedex, France*

[3]*Laboratoire Léon Brillouin, UMR 12 CNRS-CEA, Université Paris-Saclay, CEA Saclay, 91191 Gif sur Yvette Cedex, France*

(Received 13 July 2016; revised manuscript received 13 December 2016; published 25 January 2017)

The mechanism of charge motion in conductive and photosensitive mesogenic block copolymers containing polyethylene oxide (PEO) segments is investigated over a wide frequency and temperature range with the broadband dielectric spectroscopy technique. It is found that the ultraviolet (UV) irradiation, the UV intensity, and the anchoring conditions of mesogenic unit in the cells produce changes in conductivity properties and in the molecular arrangement. The anisotropic nature of the conductivity is established.

DOI: 10.1103/PhysRevE.95.012708

I. INTRODUCTION

Design and engineering of new solid polymer electrolytes (SPEs) for lithium-based batteries are among the most challenging goals for energy storage applications. Polyethylene oxide (PEO) and PEO-based derivatives are recognized as the best host matrices to dissolve lithium salts leading to a unique class of solid ionic conductors [1–3]. Charge transport mechanisms in these materials are closely related to the structural characteristics of the polymer. In amorphous polymers ($T > T_g$), a "liquid-like" conduction occurs where the random Brownian motion of macromolecular segments was considered as the driving force for cation (Li^+) transport [4]. However, the isotropic structure of the PEO matrix induces isotropic three-dimensional motions of mobile ions which can impede the overall conductivity of the material. In crystalline polymers, the crystal lattice allows a directional motion of Li^+ along fixed pathways [5] through ion hopping from one coordination site to another. If the cavity size of nanochannels formed by the PEO chains is well controlled, while keeping cations and anions separated, the ionic conductivity of crystalline SPEs can exceed that of their amorphous counterparts [6,7]. An anisotropic charge transport thus emerges as one of the key parameters to enhance the ionic conductivity of SPEs. Several investigations demonstrated that PEO-based self-assembled soft materials like liquid crystals (LCs) [8,9], polymer LCs [10,11], and surfactant mesophases [12] are good candidates for the design of anisotropic SPEs. The major importance of the microstructure of the self-assembled material for ionic transport properties and specific macromolecular architectures [13,14] or microstructure alignment techniques using magnetic fields [15,16] have been reported to enhance the effective conductivity of SPEs.

In order to get further insights into the close relationship between charge transport and structural anisotropy in PEO-based materials, lithium salt and rodlike-shaped block oligomer mixtures [Fig. 1(a)] have been designed to exhibit mesomorphic properties as well as ionic conduction capabilities [8,17]. These materials exhibit a nematic LC phase [8] in which the director **n** can be oriented in a given direction using substrates treated with alignment layers [18,19]. The anchoring energy between mesomorphic molecules and alignment layers leads to the orientation of the entire slab, providing either homogeneous or homeotropic configurations; i.e., PEO-based block oligomers are oriented either parallel or perpendicular to the substrates [18,20,21]. Using broadband dielectric spectroscopy, the conductivity of the as-prepared ionic liquid crystalline cells is studied as a function of temperature and anchoring conditions (homogeneous versus homeotropic configuration). In addition, the photoresponsive azobenzene moiety located in the central core of molecules can undergo a trans-cis conformational change upon absorption of light. The trans isomers are linear (elongated) in shape and tend to stabilize the LC order. The cis isomers, obtained under ultraviolet (UV) light irradiation, are bent and destabilize the LC mesophases to consequently modify the material properties. Ionic transport properties are investigated as a function of illumination power, which induces changes of the nematic orientational order. Based on these experimental results, it is shown that lithium salt and mesogenic oligomer mixtures could be promising materials to fabricate photoresponsive sensors to mimic biological systems such as retina.

II. MATERIALS AND METHODS

Rodlike-shaped block oligomers were prepared according to a synthetic route reported elsewhere [17]. Short terminal PEO chains were grafted on mesogenic cores containing an azobenzene moiety and bearing two types of lateral groups [methyloxy (Me) or hexyloxy (C6)] [Fig. 1(a)]. The UV-vis spectra of PEOMe and PEOC6 in CH_2Cl_2 are shown in Fig. 1(b). Three absorption bands are observed and occur at wavelengths approximatively equal to 440, 333, and 260 nm. The first transition, the lowest energy one, is assigned to an n-π^* transition. The two others are due to two different π-π^* transitions. Upon UV illumination, the intensity of the band at $\lambda = 333$ nm decreases [Fig. 1(b)] while that of $\lambda = 440$ nm increases, confirming that a trans-cis isomerization process takes place.

*corinne.binet@univ-lille1.fr

†In memoriam of our colleague Frédérick Roussel.

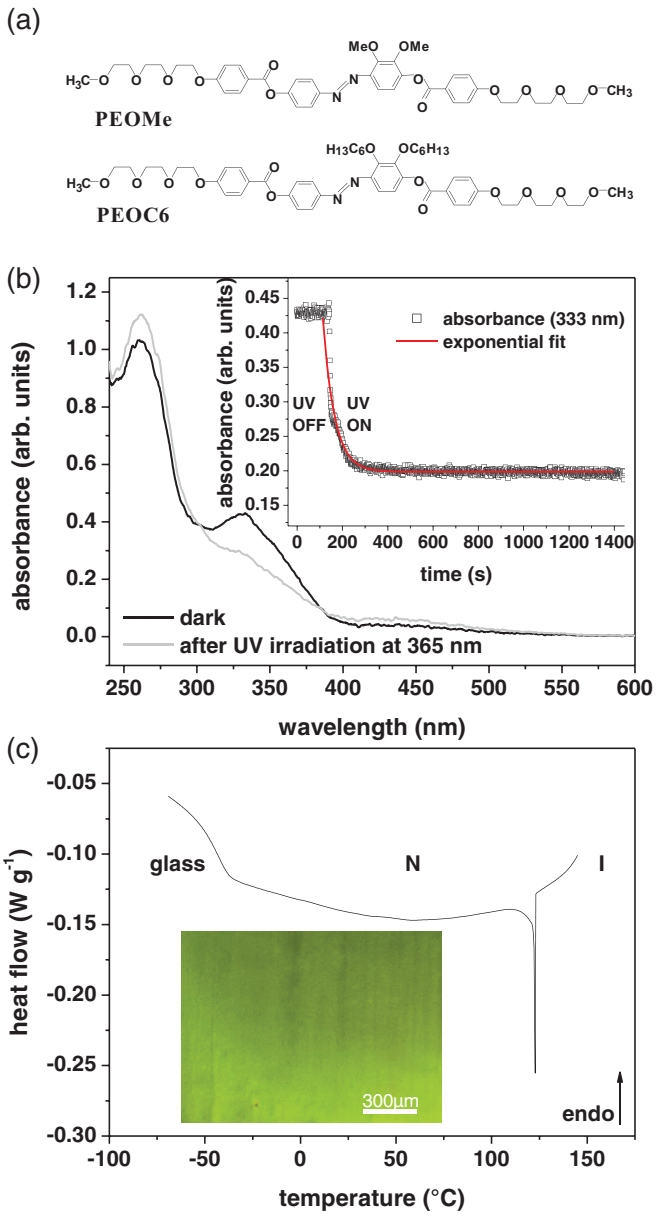

FIG. 1. (a) Chemical structure of rodlike shaped block PEO-based derivatives, (b) UV/Vis spectrum of pure PEOC6 in CH_2Cl_2 before and after UV light irradiation for 15 min at 365 nm; insert: time dependence of UV irradiation on the intensity of the $\pi - \pi^*$ transition absorption band ($\lambda = 333$ nm), (c) DSC trace of PEOC6 measured on cooling (rate 5 °C · min^{-1}); POM microphotograph ($T = 36$ °C) showing the nematic texture of PEOC6 and PEOMe in homogeneous aligned cell.

In order to obtain ionic conductors, PEOMe or PEOC6 molecules were dissolved in dry THF with either $LiN(SO_2CF_3)_2$ or $LiCF_3SO_3$ salts. Molar ratios of ethylene oxide units versus lithium cation were set at 5:1 and 5:2, respectively. After mechanical stirring of solutions followed by complete evaporation of the solvent (THF) in an oven at 100 °C for several days, the resulting mixtures were optically, thermally, and electrically characterized.

The phase behaviors of pure PEOC6 and PEOMe and their mixtures with $LiN(SO_2CF_3)_2$ or $LiCF_3SO_3$ salts were

TABLE I. Transition temperatures (°C) and phase sequence of PEOC6, PEOMe, and their mixtures with $LiN(SO_2CF_3)_2$ or $LiCF_3SO_3$ salts measured on cooling (5 °C · min^{-1}) by DSC and observed by polarized optical microscopy. Abbreviations: I, isotropic; N, nematic.

	PEOC6 $I \leftrightarrow \mathbf{N} \leftrightarrow$ Glass [° C]		PEOMe $I \leftrightarrow \mathbf{N} \leftrightarrow$ Glass [° C]	
No salt	123.2	−37	166	−30
0.2 $LiN(SO_2CF_3)_2$	60	−40	143	−16
0.4 $LiCF_3SO_3$	50.9	−36		n/a

studied by polarized optical microscopy (Olympus BX60) equipped with a Linkam LTS420 stage and differential scanning calorimetry (Q2000, TA Instrument). All samples exhibit a nematic phase with a typical texture in planar (homogeneous) cell [Fig. 1(c)] which can be easily frozen out upon cooling as shown by the heat capacity step (glass transition) observed by DSC at low temperature. Transition temperatures and phase sequences are reported in Table I. The difference in T_g values of pure compounds is probably due to the size of the pendant substituents attached to the mesogenic core. The length of the hexyl group is higher than for the methyl group, and as a consequence the free volume of the C6 is increased and the T_g could be slightly decreased compared to compounds with Me. It is very hard to discuss the T_g of lithium salt mixtures because the concentrations and the mobility of salt change.

A 200 W Hg arc lamp (Lot Oriel, France) was used to perform the UV light irradiations. An optical fiber was employed to shine the sample placed in the Linkam hot stage. An anticalorific filter was used to avoid infrared heating of the sample. Interferential filters were set to adjust the wavelength of the beam inducing the trans-cis isomerization of the azobenzene moiety. Density filters were used to have the suitable UV intensity. The UV intensity was checked with a Nova II power meter (Ophir, USA).

For dielectric measurements, materials were introduced by means of capillarity action at $T > T_I$ (isotropic temperature) into 15 µm thick planar or homeotropic commercial cells (EHC Inc., Japan or AWAT, Poland). The glass plates of both commercial cells are coated on their inner surface, first with an indium tin oxide (ITO) transparent conducting layer (resistivity 10Ω/□), and, second, with a rubbed, polyimide (PI) alignment layer. The type of PI alignment layer depends on the desired anchoring: a homogeneous (planar) one or a homeotropic one.

Broadband dielectric spectroscopy (BDS) measurements were carried out on a ModuLab-MTS test system (Solartron Analytical, Ametek) in the frequency range 0.01 Hz–1 MHz. The amplitude of the oscillating voltage was set to 10 mV, and the temperature of the sample was controlled with a Linkam LTS420 stage. BDS measures the complex dielectric function (ε^*), which is equivalent to the complex electrical conductivity function (σ^*) because $\sigma^* = j\varepsilon_0\omega\varepsilon^*$ where ω is the angular frequency and ε_0 is the vacuum permittivity constant. This

complex electrical conductivity σ^* can be again written as

$$\sigma^*(\omega) = \sigma'(\omega) + j\sigma''(\omega). \quad (1)$$

The real part of σ^* is linked to the imaginary part of the complex dielectric permittivity through the relation $\mathrm{Re}(\sigma^*) = (\omega\varepsilon_0)\mathrm{Im}(\varepsilon^*)$ with $\mathrm{Im}(\varepsilon^*) = \varepsilon''$ consequently $\sigma' = \varepsilon_0\omega\varepsilon''$ [22,23].

To analyze the frequency dependence of the complex conductivity, different models have been used like Cole-Cole [24], Cole-Davidson, or Kohlrausch-Williams-Watts [25] functions beforehand transformed into their conductivity representations. Jonscher proposed a power-law model [26] later modified by Almond and coworkers [27] to analyze the real part of the complex conductivity, but it seems to lack a physical basis [28]. Dyre developed a theoretical approach [29], the random free energy barrier model, which assumes that the conduction occurs with charge carriers hopping in a random spatially varying potential landscape. An analytical solution is obtained with a continuous-time-random-walk approximation, and the complex conductivity is described by Eq. (2) and used in the frame of this study to analyze the charge transport-dominated regime in the bulk of our samples:

$$\sigma^*(\omega) = \sigma_{DC} * \left[\frac{i\omega\tau_e}{\ln(1 + i\omega\tau_e)}\right], \quad (2)$$

τ_e is the characteristic time (or hopping time) related to the attempt frequency to overcome the largest energy barrier determining the direct current conductivity σ_{DC}.

The real part and the imaginary part of the complex conductivity can be expressed [Eq. (3)], and the experimental data will be simultaneously fitted:

$$\sigma'(\omega) = \frac{\sigma_{DC}\omega\tau_e \arctan(\omega\tau_e)}{\frac{1}{4}\ln^2[1 + (\omega\tau_e)^2] + [\arctan(\omega\tau_e)]^2},$$

$$\sigma''(\omega) = \frac{\sigma_{DC}\omega\tau_e \ln[1 + (\omega\tau_e)^2]}{\frac{1}{2}\ln^2[1 + (\omega\tau_e)^2] + 2[\arctan(\omega\tau_e)]^2}. \quad (3)$$

The Dyre approach has been often used in disordered ion-conducting solids and ionic liquids to describe the transport of charge carriers [30,31].

Dielectric measurements were also performed under UV light irradiation for the different ionic LC systems and anchoring treatments. The cell sample was illuminated during about 10 000 s, and simultaneously the corresponding dielectric spectra were recorded with a "scanning loop" (every 30 s). After each UV intensity, the sample cell was (1) heated in the dark to the isotropic state kept warm during 15 min and then (2) was slowly cooled (0.5 °C/min) to the studied temperature and kept warm for more than 8 hr before beginning a new UV intensity experiment. The study is realized from low UV intensities to higher intensities. This procedure is expected to favor a good alignment of material and minimize a memory effect of the cell.

III. RESULTS AND DISCUSSION

Figure 2 shows the frequency dependence of both the complex conductivity (σ^*) and complex dielectric function (ε^*) for the mixture PEOC6:$LiCF_3SO_3$ (5:2) recorded at temperatures ranging from −26 to +50 °C with homogeneously aligned cells. This figure is divided into plots of $\sigma'(f)$,$\sigma''(f)$,$\varepsilon'(f)$, and $\varepsilon''(f)$. For a fixed temperature, three frequency domains can be observed in the real part of the complex conductivity spectra. At low frequencies electrode polarization effects dominate (marked by a peak in the σ'' plot). This phenomenon is likely due to the blocking effect of the charge carriers and could be induced by the formation of electrical double layers, which could retard the charge transport. At intermediate frequencies, σ' exhibits a plateau-like behavior corresponding to the DC conductivity contribution (related to the linear dependence of slope 1 in the ε'' plot). At higher frequencies, a subdiffusive conductivity domain is observed [22]. Indeed, the AC conductivity $\sigma'(f)$ is independent on a large range frequency (plateau zone) of the electric field frequency, and drastically increases above a characteristic onset frequency. At this particular frequency the ε' plot presents a step.

In this work we have focused our attention on the plateau and the subdiffusive region because the most relevant parameters for the electrical characterization of electrolytes are the value of the DC conductivity (σ_{DC}) and the hopping frequency [$f_e = \omega_e/2\pi = 1/(2\pi\tau_e)$], which can be determined from fitting the experimental data to Eq. (3). A good agreement is found between measurements (symbols) and fits (solid lines) except below −14 °C where a small discrepancy is observed at high frequencies. One can think of two possible explanations to understand this effect. On the one hand, when the temperature decreases, the plateau region and the subdiffusive region shift toward lower frequencies; consequently at the smallest temperatures in the ε'' plot we can now observe the beginning of the left side of the relaxation peak (related to the ITO coating of the electrodes) with a very small amplitude previously masked by the charge transport phenomenon. This relaxation peak disturbs the fit. On the other hand, the vicinity of the glass transition temperature of the sample ($T_g = -36$ °C) could affect the diffusion process of carriers and in turn modify the charge transport properties.

To get further insights, experimental data were normalized with respect to σ_{DC} and f_e [Fig. 3(a)] leading to the overlap of all data sets recorded at various temperatures. This shows that both electrode polarization and bulk charge transport exhibit a similar thermal activation process; i.e., different phenomena observed in two distinct spectral regions are governed by the same underlying mechanism.

A linear dependency has been found between the DC conductivity (σ_{DC}) and the critical radial frequency ω_e as shown in Fig. 3(b). This finding is known as the Barton-Nakajima-Namikawa (BNN) relationship [32]. It indicates that the DC and AC conductivities are closely related to each other and based on the same mechanism of charge transport.

The temperature dependence of the hopping frequency of charge carriers provides useful information on ion migration dynamics in the sample. From Fig. 3(c), both ω_e and σ_{DC} values decrease with decreasing temperature. But their evolutions as a function of the inverse temperature or the temperature follow a nonlinear, i.e., non-Arrhenius-like, behavior. According to these observations, the experimental

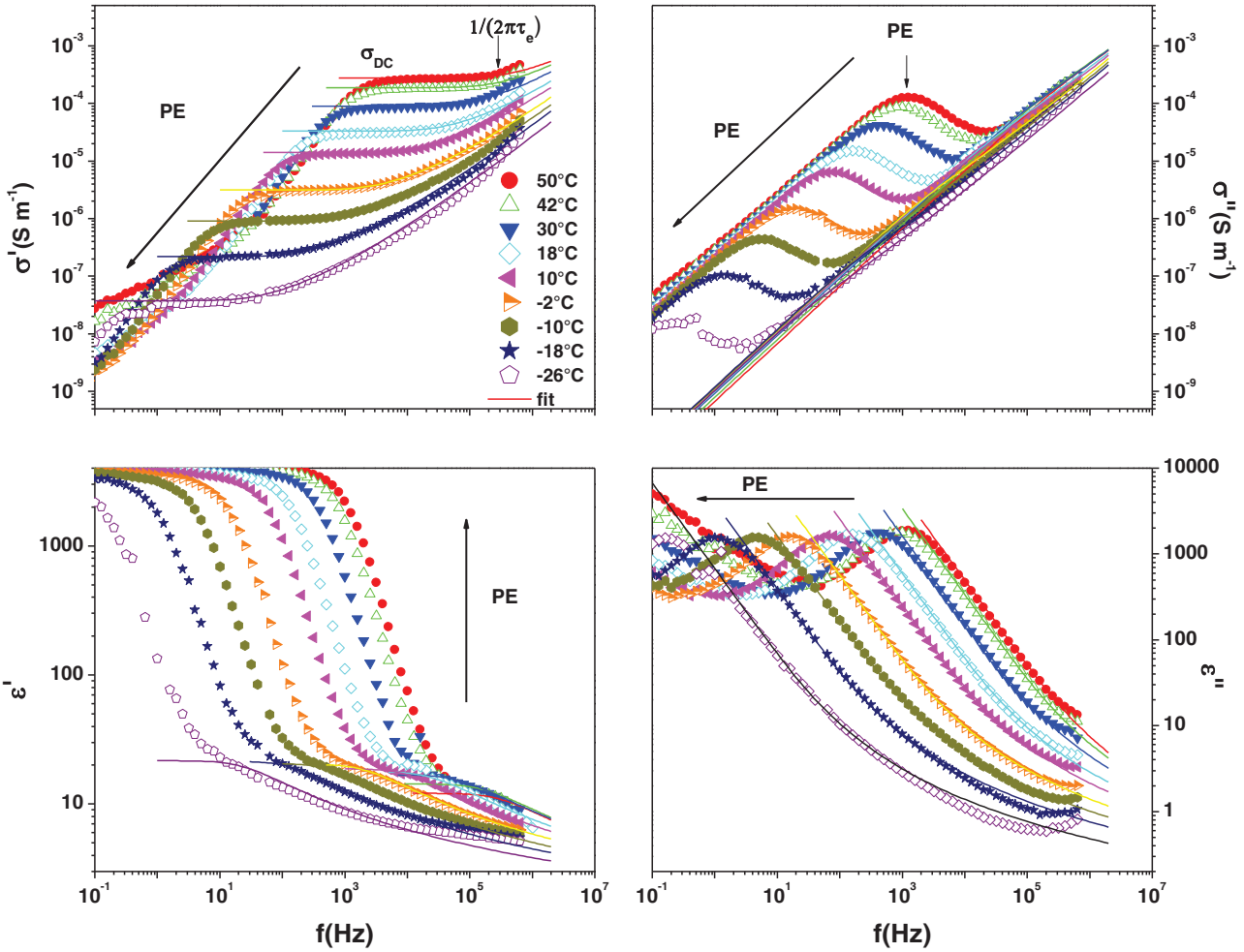

FIG. 2. Frequency dependences of the complex conductivity and the complex dielectric function for PEOC6:$LiCF_3SO_3$ (5:2) at different temperatures; symbols are experimental data points, and solid lines are the best fit curves obtained with the theoretical approach developed by Dyre. The error bars are comparable to the size of the symbols. Attention is paid to the charge transport processes (fitted part of curves) even if electrode polarization (PE) effects occur on the low-frequency side.

data were fitted with a modified Vogel-Fulcher-Tammann (VFT) equation. This model is usually employed to describe the temperature dependence of physical parameters (X) of glass-forming systems and/or electrolytes [33]:

$$X(T) = \frac{X_0}{\sqrt{T}} e^{-E/k(T-T_0)}, \tag{4}$$

where X_0 is a constant, k the Boltzmann constant, E the activation energy, and T_0 the thermodynamic ideal glass transition temperature.

Figure 3(c) shows that the modified VFT equation is able to reproduce experimental data as observed in previous works on ionic liquids [34]. The both VFT dependencies run almost parallel, meaning that ω_e has almost the same activation energy as σ_{DC}.

Figure 4 shows the evolution of σ_{DC} as a function of inverse temperature ($1000/T$) and temperature (T) for both PEOMe and PEOC6 molecules undoped or doped with various alkali salts and having a planar alignment. Compared with pure compounds, mixtures prepared with Li salts exhibit a significant enhancement of σ_{DC} at room temperature (T = 30 °C) by at least three orders of magnitude. Indeed, the pure mesomorphic materials are neutral molecules, and then their ionic conductivity should be zero. The very low level of ionic conductivity which is measured is probably due to remaining impurities or traces of water. The doping with lithium salts is then mandatory to achieve a reasonable level of ionic conductivities through the long-range transport mechanisms of ions.

The temperature dependence of σ_{DC} shows that the ionic conductivity is thermally activated and follows a VFT process [Eq. (4); fitting parameters are summarized in Table II) indicating that a cooperative charge transport mechanism takes place where PEO chains are involved in the carrier motion. It is noteworthy that $\sigma_{DC}(T)$ of doped samples exhibit similar values regardless of molecular architecture of the host (PEOMe vs PEOC6) and fraction and nature of lithium salts (size and type of counter-anion). This result indicates that (1) the ionic conduction process is essentially dominated by ionic species and (2) the ion mobility is only slightly affected by the length of the lateral chain grafted on the mesogenic cores. At high temperature, a deviation of the experimental data from the VFT equation reveals a change in the temperature dependence of the electrical conductivity which slightly decreases or levels off. This result can be related to the evolution of the

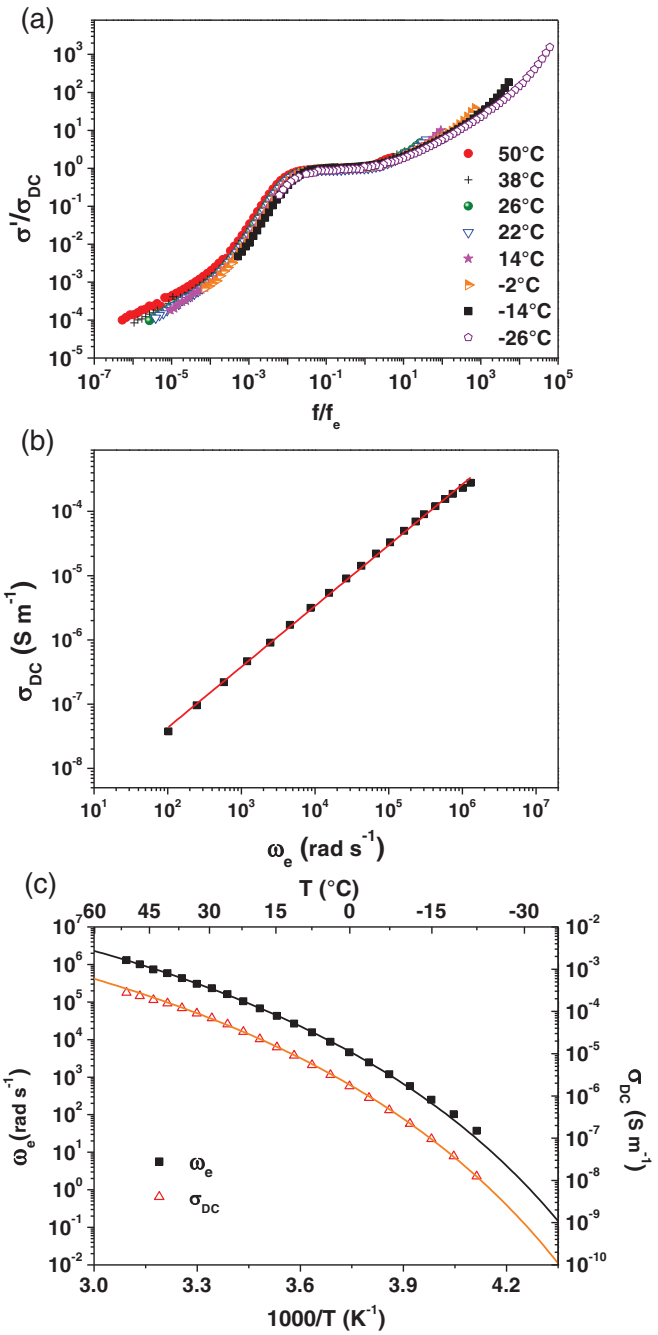

FIG. 3. (a) Normalized plots of the real part of the complex conductivity versus normalized frequency scaling with respect to temperature for PEOC6:$LiCF_3SO_3$ (5:2). (b) BNN plot σ_{DC} versus ω_e; the line is a linear regression to these data. (c) Temperature dependence and inverse temperature dependence of the hopping radial frequency ω_e and the DC conductivity. The continuous solid line represents the fit of experimental data to Eq. (3) [obtained fit values are for hopping radial frequency curve: $\omega_{e0} = 2.1(\pm 0.5) \times 10^{11}\mathrm{K}^{0.5} \cdot \mathrm{rad}\cdot\mathrm{s}^{-1}, E = 11\,100 \pm 300\,\mathrm{J}\cdot\mathrm{mol}$ and $T_0 = 177 \pm 4\mathrm{K}$, and for DC conductivity: $\sigma_{DC0} = 32 \pm 5\mathrm{K}^{0.5} \cdot \mathrm{S} \cdot \mathrm{m}^{-1}, E = 10\,400 \pm 300\,\mathrm{J}\cdot\mathrm{mol}$ and $T_0 = 177 \pm 4\,\mathrm{K}$].

orientational order parameter of the LC phase near the nematic to isotropic transition [35]. This phenomenon is seen more particularly in the PEOMe salt because for this experiment the temperatures go 15 °C higher than the isotropic transition

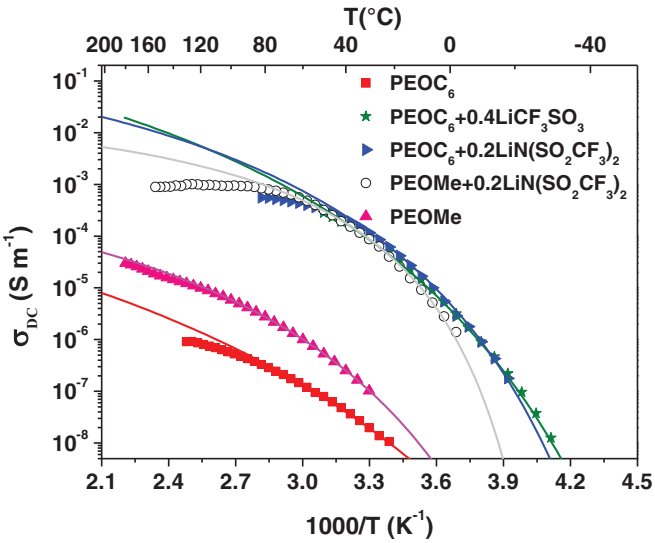

FIG. 4. Temperature dependence and inverse temperature dependence of DC conductivity σ_{DC} of pure PEO or doped PEO. Symbols are experimental data points and solid lines are the best fit curves to modified Vogel-Fulcher-Tammann equation [Eq. (4)].

temperature whereas the other curves stop just at the isotropic temperature. In other words, the change of the local structure from anisotropic to isotropic modifies the transport properties of the materials leading to a decrease of their electrical conductivity in the vicinity of the isotropic state.

Due to the presence of a double bond N = N in the chemical structure of studied LC molecules, a trans-cis photochemical isomerization may be induced in the samples by UV irradiation as shown in Fig. 1(b). The irradiation impact on the DC conductivity is reported in Fig. 5 for a PEOC6:$LiN(SO_2CF_3)_2$ (5:1) cell treated with a homogenous alignment. The excited wavelength is 365 nm ± 2 nm. Figure 5(a) shows the obtained DC conductivity versus irradiation time for different UV intensities at 30 °C. Whatever the value of the UV intensity, the curves decrease and then level off after some period of irradiation, indicating that a photostationary state is reached. To explain this behavior, it could be suggested that the photoinduced cis configuration (bended form) disturbs the mesophase, which reduces the order of the nematic phase and consequently lessens the value of the DC conductivity. Due to its geometry, the bended form could act as a trap for Li^+ cations and could prevent ion mobility.

From Fig. 5(a) we can also note that when UV intensity is increased, the decrease of the DC conductivity is more important during the experiment time. Moreover with some repeated UV exposures, the sensitivity of the cell decreases and hence also the initial value of the DC conductivity. To understand this effect, the percentage of loss of DC conductivity during the experiment is represented in the insert of Fig. 5(a). This parameter is calculated by the following ratio:

$$\sigma_{\mathrm{loss}} = \frac{\sigma_{\mathrm{dark}} - \sigma_{\mathrm{end}}}{\sigma_{\mathrm{dark}}}, \tag{5}$$

where σ_{dark} is the DC conductivity before irradiation (time = 0) and σ_{end} is the DC conductivity under UV irradiation at the end of the experiment. On the one hand, it appears that the

TABLE II. Fitted parameters concerning the temperature dependence of DC conductivity curves (Fig. 4) obtained with Eq. (4) and glass transition temperature (T_g) of pure PEO or PEO doped with different lithium salts.

Name	Salt	σ_{DC0} ($K^{1/2}S \cdot m^{-1}$)	$\Delta\sigma_{DC0}$ ($K^{1/2}S \cdot m^{-1}$)	E ($J \cdot mol$)	ΔE ($J \cdot mol$)	T_0 (K)	ΔT_0 (K)	T_g (K)
$PEOC_6$	Pure	0.032	0.054	13 781	4521	158.6	25.6	236
$PEOC_6$	0.4 $LiCF_3SO_3$	31.95	5.0	10 375	313	177.2	4.4	237
$PEOC_6$	0.2 $LiN(SO_2CF_3)_2$	13.7	4.8	8119	582	192.0	3.5	233
PEOMe	0.2 $LiN(SO_2CF_3)_2$	0.779	0.056	3945	102	227.1	4.2	257
PEOMe	Pure	0.043	0.008	8415	406	202.9	2.9	243

DC conductivity losses are smaller when the UV intensity is low. On the other hand, this curve highlights the existence of a threshold effect in UV light intensity on conductivity behavior. The critical value in regard to experimental conditions is around $3mW \cdot cm^{-2}$. Below this intensity the loss percentage of conductivity seems to grow linearly, while above this value it reaches a plateau found around 18%, which is the same order of magnitude as quantum efficiency (spectral sensitivity) of CCD sensors (e.g., "blue plus" of Olympus society [36]) at the same wavelength (UV). It appears that a threshold is measured for an irradiation of $3mW \cdot cm^2$. Such surface specific power is required to complete the photoisomerization of all molecules in the cell, while below this critical value, the photochemical reaction has a very low yield.

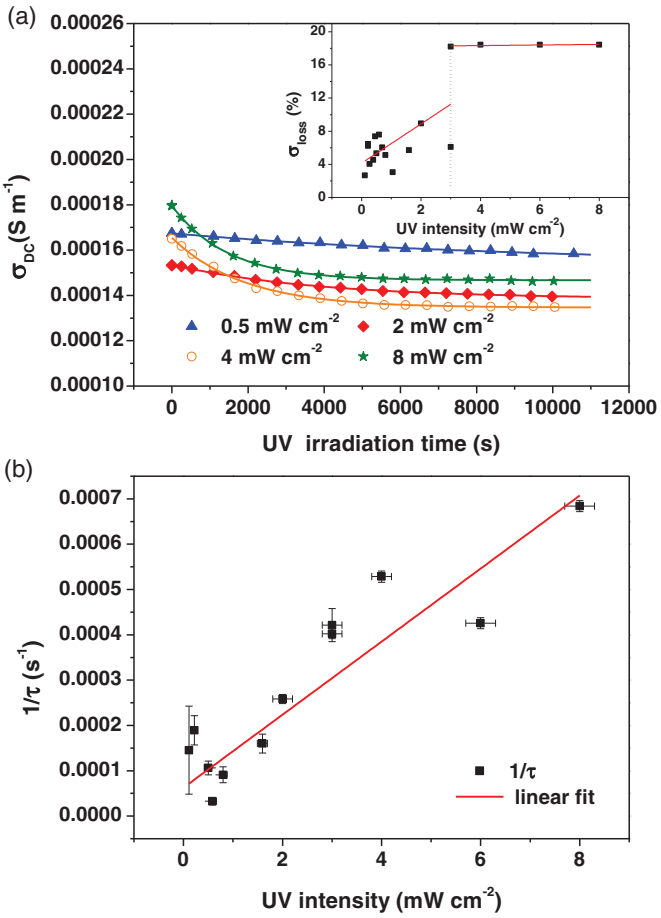

FIG. 5. Influence of UV irradiation (365 nm) under various intensities for PEOC6:$LiN(SO_2CF_3)_2$ (5:1) into a homogenous cell at 30 °C: (a) time dependence of the DC conductivity, insert percentage of loss of conductivity obtained with Eq. (5). Symbols are experimental data points and solid lines are the best fit curves to Eq. (6). (b) Rate constant ($1/\tau$) of the process versus UV intensity.

In order to estimate the time decay or the evolution of DC conductivity, the σ_{DC} data as function of the irradiation time have been fitted with an exponential rate law:

$$\sigma_{DC} = A\exp\left(-\frac{t}{\tau}\right) + \sigma_{\infty}, \tag{6}$$

where the fit parameter σ_{∞} is assumed to be equal to σ_{end}, A is linked to the amplitude modulation induced by UV irradiation in σ_{DC} values, and τ is the characteristic decay time of the process. The solid lines in the conductivity spectra versus irradiation time denote the fits of experimental data obtained with Eq. (6).

Figure 5(b) shows a rather linear evolution of the rate constant ($1/\tau$) of the process versus UV intensity. Previously a threshold effect in terms of loss of conductivity and a stabilization of the conductivity under illumination have been described. It would seem that the establishment of this final photostationary state is accelerated by the UV power: the higher the UV intensity is, the faster the kinetic of isomerization occurs.

As established above an anisotropic phase and the control of the molecular ordering inside this phase play an important role on the conductivity. To highlight this crucial observation, the organization and orientation of the nematic phase were changed by altering the anchoring conditions using Awat commercial cells (homogeneous versus homeotropic configuration). The temperature dependence of DC conductivity for PEOMe: $LiN(SO_2CF_3)_2$ (5:1) for both configurations is presented in Fig. 6(a) as well as their evolutions under UV irradiation. To compare the behavior with and without UV irradiation, the percentage of loss of DC conductivity ($\frac{\sigma_{dark}-\sigma_{UV}}{\sigma_{dark}}$) is calculated at a reduced temperature $T/T_{NI} = 0.58$ (84 °C) and is shown in Fig. 6(b). For both configurations the DC conductivity curves look similar and follow a VFT-like temperature dependence, as evidenced previously. The planar orientation of cell favors the ionic conductivity and demonstrates well the anisotropic dependence of conductivity. To explain this behavior, a mechanism could be proposed linked to the average coordinance mode of Li^+ cation. Molecular dynamics simulations suggest that the Li^+ ions are complexed to PEO through approximately five ether oxygens of the PEO chain [37], while only three are available on our peculiar mesogenic molecules. Consequently, the mobility of the Li^+ cations and the DC conductivity will be governed by

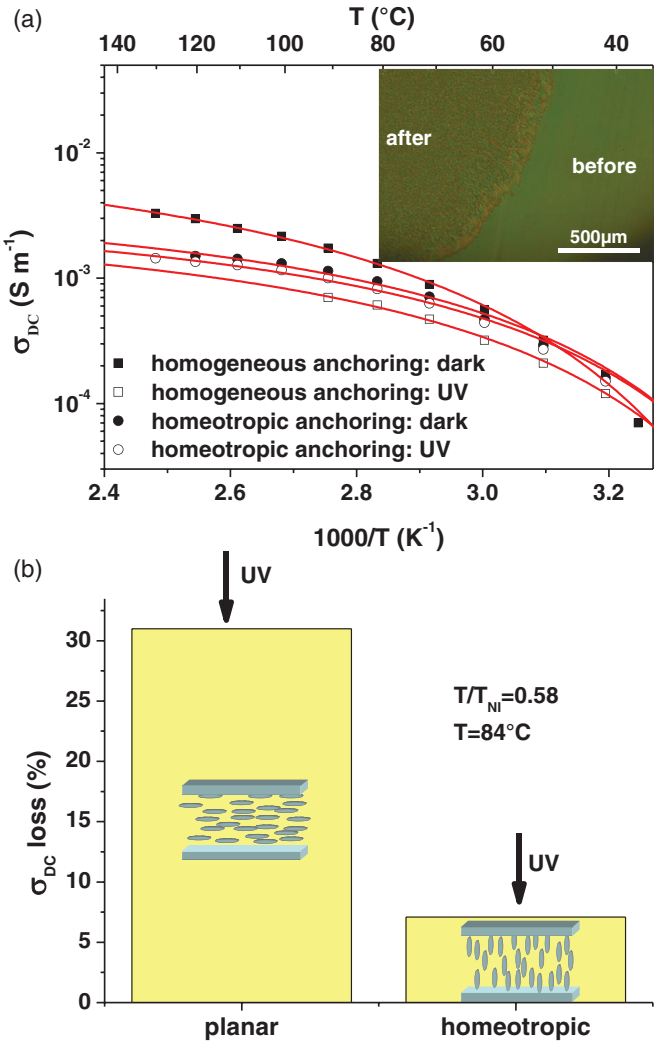

FIG. 6. Influence of anchoring: (a) Temperature dependence and inversed temperature dependence of ionic conductivity for PEOMe:LiN$(SO_2CF_3)_2$ (5:1) for a homogenous or homeotropic anchoring with or without UV irradiation. The solid lines represent the fit of experimental data to the modified VFT equation. The optical micrograph for a homogeneous anchoring before and after UV irradiation, (b) Percentage of DC conductivity loss when UV light is switched on for a reduced temperature T/T_{NI} equal to 0.58.

the motion of the cations between complexation sites assisted by the segmental motion of the PEO moieties [38]. A hopping mechanism of cations between mesogenic units of the LC matrix is then expected as it was deduced previously from NMR experiments [8]. Based on these previous studies and findings, we could propose a possible explanation for the fact that the σ_{DC} values with a homogeneous anchoring of the cell are higher than the σ_{DC} values with a homeotropic anchoring of cell. Without UV irradiation, in the case of planar anchoring, the lithium ion transport in a perpendicular direction to the long axis of a molecule could be facilitated because of the vicinity of PEO chains with which the cations will be associated. Li^+ could easily move from its associated PEO chain to the next adjacent parallel PEO chain via simple rotation motion [Fig. 7(a)]. The long-range motion occurs from the repetition of such elementary steps. In the

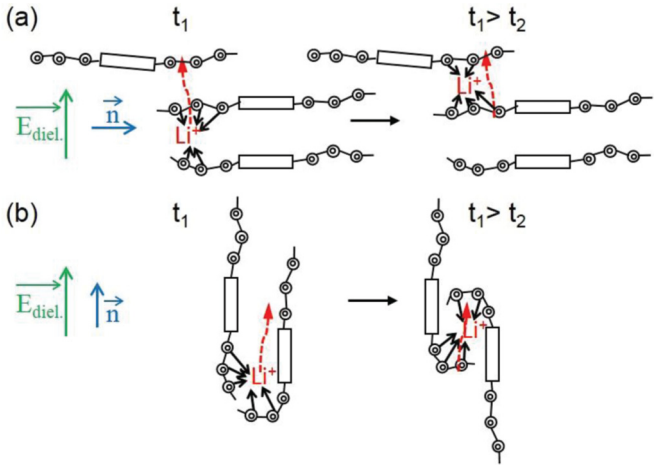

FIG. 7. Schematic of the segmental motion assisted diffusion of Li^+ between the PEO moieties of different molecules for a planar (a) and a homeotropic (b) anchoring. The circles and the rectangles, respectively, represent the ether oxygens of PEO chains and the mesogenic blocks of the molecules.

homeotropic case, to move the Li^+ ion might be transported parallel to the long axis of the mesogenic molecules. There again, the cation transport might be preferentially between two adjacent PEO chains. Efficient transport might occur for large motion and significant distortion of the PEO chain or for concerted transport of the cations within the mesogenic unit [Fig. 7(b)]. This translation movement is more difficult to operate than a simple rotation, which would explain the higher conductivity values for a planar anchoring of the cell. The suggested conduction mechanism could also corroborate the fact that whatever the nematic electrolyte is, for a same cell configuration, a planar one in Fig. 4, the conductivity values would be quite close.

With UV irradiation, the conductivity values decrease whatever the cell configuration. However, the phenomenon is more marked in the case of a homogeneous anchoring and increased with high temperatures. For example, at 84 °C the DC conductivity loss percentage is 30% for planar alignment and only 8% for homeotropic one. In homeotropic configuration, the director **n** of the nematic phase is parallel to the direction of propagation of UV wave limiting interaction with azobenzene moiety, whereas, in the planar configuration, the N = N bound is globally perpendicular to the direction of propagation of the UV wave, which favors the interaction between the wave and the molecule. In Fig. 6(a) the polarized optical microphotograph obtained with a homogeneous anchoring of the cell shows clearly that the UV irradiation destroys the initial order. Before irradiation a well-ordered nematic texture is obtained, and just after UV irradiation a black area appears, which is the proof of either an isotropic transition [39] or of a photoalignment during UV irradiation. After 2 hr relaxation time of the irradiated part of the sample, this black area looks like a Schlieren nematic texture, i.e., a disoriented texture.

IV. CONCLUSION

The present study has shown that the bulk conductive properties of these photonematic LC salt materials are strongly

affected by the temperature, the UV irradiation, and the anchoring conditions. These materials also present an important electrode polarization on the low-frequency side, which it would be interesting to further investigate [40,41].

The temperature dependence of conductivity is found to be governed by a noncooperative mode and follows a VFT behavior. An exponential decreasing of DC conductivity values results from the UV light application due to the trans-cis isomerization of PEO chains and to a loss of order in the nematic phase. Under increasing light intensities the rate constant linked to the isomerization process seems to follow a linear law. In addition anchoring treatment of the cell surface allows alignment of molecules and influences the bulk conductivity. The DC conductivity obtained with a planar anchoring is higher than that determined with a homeotropic anchoring and confirms the conductivity anisotropy. For both geometries, the conductivity is reduced under photo-irradiation and shows the possibility of obtaining photoresponsive electrolytes.

[1] M. B. Armand, in *Fast Ion Transport in Solids*, edited by W. Van Gool (North-Holland, Amsterdam, 1973), p. 665.

[2] M. B. Armand, J. M. Chabango, and M. J. Duclot, in *Fast Ion Transport in Solids*, edited by P. Vashishta, J. N. Mundy, and G. K. Shenoy (North-Holland, Amsterdam, 1979), p. 131.

[3] D. E. Fenton, J. M. Parker, and P. V. Wright, Polymer **14**, 589 (1973).

[4] M. A. Ratner and D. F. Shriver, Chem. Rev. **88**, 109 (1988).

[5] C. Zhang, S. Gamble, D. Ainsworth, A. M. Z. Slawin, Y. G. Andreev, and P. G. Bruce, Nat. Mater. **8**, 580 (2009).

[6] A. M. Christie, S. J. Lilley, E. Staunton, Y. G. Andreev, and P. G. Bruce, Nature (London) **433**, 50 (2005).

[7] L.-Y. Yang, D.-X. Wei, M. Xu, Y.-F. Yao, and Q. Chen, Angew. Chem. Int. Ed. **53**, 3631 (2014).

[8] P. Judeinstein and F. Roussel, Adv. Mater. **17**, 723 (2005).

[9] K. Goossens, K. Lava, C.W. Bielawski, and K. Binnemans, Chem. Rev. **116**, 4643 (2016).

[10] K. Kishimoto, M. Yoshio, T. Mukai, M. Yoshizawa, H. Ohno, and T. Kato, J. Am. Chem. Soc. **125**, 3196 (2003).

[11] J. Li, K. Kamata, M. Komura, T. Yamada, H. Yoshida, and T. Iyoda, Macromolecules **40**, 8125 (2007).

[12] M. Yoshio, T. Kagata, K. Hoshino, T. Mukai, H. Ohno, and T. Kato, J. Am. Chem. Soc. **128**, 5570 (2006).

[13] D. Golodnitsky, E. Livshits, R. Kovarsky, E. Peled, S. H. Chung, S. Suarez, and S. G. Greenbaum, Electrochem. Solid-State Lett. **7**, A412 (2004).

[14] D. M. Smith, B. Dong, R. W. Marron, M. J. Birnkrant, Y. A. Elabd, L. V. Natarajan, V. P. Tondiglia, T. J. Bunning, and C. Y. Li, Nano. Lett. **12**, 310 (2012).

[15] P. W. Majewski, M. Gopinadhan, and C. O. Osuji, Soft Matter **9**, 7106 (2013).

[16] P. Judeinstein, S. Huet, and P. Lesot, RSC Adv. **3**, 16604 (2013).

[17] P. Judeinstein, P. Berdague, J. P. Bayle, N. Sinha, and K. V. Ramanathan, Liq. Cryst. **28**, 1691 (2001).

[18] I. C. Khoo and S. T. Wu, *Optics and Nonlinear Optics of Liquid Crystals* (World Scientific, Singapore, 1993).

[19] F. Roussel, J.-F. Brun, A. Allart, L. Huang, and S. O'Brien, AIP Adv. **2**, 012110 (2012).

[20] F. Roussel and B. M. Fung, Phys. Rev. E **67**, 041709 (2003).

[21] M. Boussoualem, M. Ismaili, and F. Roussel, Soft Matter **10**, 367 (2014).

[22] J. Leys, M. Wübbenhorst, C. Preethy Menon, R. Rajesh, J. Thoen, C. Glorieux, P. Nockemann, B. Thijs, K. Binnemans, and S. Longuemart, J. Chem. Phys. **128**, 0645091 (2008).

[23] F. Kremer and A. Schönhals (eds.), *Broadband Dielectric Spectrocopy* (Springer Verlag, Berlin, Heidelberg, 2003).

[24] J. R. Macdonald and G. B. Cook, J. Electroanal. Chem **193**, 57 (1985).

[25] C. T. Moynihan, J. Non-Cryst. Solids **172-174**, 1395 (1994).

[26] A. K. Jonscher, Nature (London) **267**, 673 (1977).

[27] D. P. Almond, G. K. Duncan, and A. R. West, Solid State Ionics **8**, 159 (1983).

[28] J. R. Macdonald, Solid State Ionics **133**, 79 (2000).

[29] J. C. Dyre, J. Appl. Phys. **64**, 2456 (1988).

[30] J. R. Sangoro, A. Serghei, S. Naumov, P. Galvosas, J. Kärger, C. Wespe, F. Bordusa, and F. Kremer, Phys. Rev. E **77**, 051202 (2008).

[31] J. R. Sangaro and F. Kremer, Acc. Chem. Res. **45**, 525 (2012).

[32] J. C. Dyre and T. B. Schrøder, Rev. Mod. Phys. **72**, 873 (2000).

[33] V. Di Noto, D. Longo, and V. Münchow, J. Phys. Chem. B **103**, 2636 (1999).

[34] C. Iacob, J. R. Sangoro, P. Papadopoulos, T. Schubert, S. Naumov, R. Valiullin, J. Kärger, and F. Kremer, Phys. Chem. Chem. Phys. **12**, 13798 (2010).

[35] V. Popa-Nita, I. Gerlic, and S. Kralj, Int. J. Mol. Sci. **10**, 3971 (2009).

[36] http://olympus.magnet.fsu.edu/primer/digitalimaging/concepts/quantumefficiency.html.

[37] F. Müller-Plathe and W. F. Van Gunsteren, J. Chem. Phys. **103**, 4745 (1995).

[38] W. H. Meyer, Adv. Mater. **10**, 439 (1998).

[39] H. Tokuhisa, M. Yokoyama, and K. Kimura, Chem. Mater **5**, 989 (1993).

[40] A. Serghei, M. Tress, J. R. Sangoro, and F. Kremer, Phys. Rev. B **80**, 184301 (2009).

[41] M. Samet, V. Levchenko, G. Boiteux, G. Seytre, A. Kallel, and A. Serghei, J. Chem. Phys. **142**, 194703 (2015).